Published in final edited form as:
Phys Chem Chem Phys. 2022 September 06; 24(39): 24021–24031. doi:10.1039/d2cp03064k.

Inferring entropy production rate from partially observed Langevin dynamics under coarse-graining†

Aishani Ghosal[a], **Gili Bisker**[a,b,c,d,*]

[a]Department of Biomedical Engineering, Tel Aviv University, Tel Aviv 6997801, Israel

[b]Center for Physics and Chemistry of Living Systems, Tel-Aviv University, Tel Aviv 6997801, Israel

[c]Center for Nanoscience and Nanotechnology, Tel-Aviv University, Tel Aviv 6997801, Israel

[d]Center for Light-Matter Interaction, Tel-Aviv University, Tel Aviv 6997801, Israel

Abstract

The entropy production rate (EPR) measures time-irreversibility in systems operating far from equilibrium. The challenge in estimating the EPR for a continuous variable system is the finite spatiotemporal resolution and the limited accessibility to all of the nonequilibrium degrees of freedom. Here, we estimate the irreversibility in partially observed systems following oscillatory dynamics governed by coupled overdamped Langevin equations. We coarse-grain an observed variable of a nonequilibrium driven system into a few discrete states and estimate a lower bound on the total EPR. As a model system, we use hair-cell bundle oscillations driven by molecular motors, such that the bundle tip position is observed, but the positions of the motors are hidden. In the observed variable space, the underlying driven process exhibits second-order semi-Markov statistics. The waiting time distributions (WTD), associated with transitions among the coarse-grained states, are non-exponential and convey the information on the broken time-reversal symmetry. By invoking the underlying time-irreversibility, we calculate a lower bound on the total EPR from the Kullback–Leibler divergence (KLD) between WTD. We show that the mean dwell-time asymmetry factor – the ratio between the mean dwell-times along the forward direction and the backward direction, can qualitatively measure the degree of broken time reversal symmetry and increases with finer spatial resolution. Finally, we apply our methodology to a continuous-time discrete Markov chain model, coarse-grained into a linear system exhibiting second-order semi-Markovian statistics, and demonstrate the estimation of a lower bound on the total EPR from irreversibility manifested only in the WTD.

†Electronic supplementary information (ESI) available. See DOI: https://doi.org/10.1039/d2cp03064k

bisker@tauex.tau.ac.il .

Author contributions

A. G. and G. B. designed research, performed research, analysed data, and wrote the paper.

Conflicts of interest

There are no conflicts to declare.

Europe PMC Funders Author Manuscripts

1 Introduction

Irreversible processes in living systems lead to the production of entropy, which is a measure of energy dissipation and a signature of the arrow of time.[1–5] Quantifying the entropy production can shed light on the underlying nonequilibrium dynamics and provide insights into the thermodynamic burden of biological processes.[6–8] There are primarily two methods to infer that a system is out-of-equilibrium: (i) invasive methods,[9–12] and (ii) non-invasive[13–16] methods. In invasive methods, the system's response to a perturbation is measured following an external manipulation, and the violation of the fluctuation–dissipation theorem (FDT)[9,17–22] confirms the nonequilibrium nature of the underlying process. On the other hand, non-invasive methods do not require a direct perturbation to a system, and can detect the nonequilibrium nature of the process from various system properties, such as broken time-reversal symmetry,[23,24] presence of net probability current of observables,[7,13,16,25–29] or asymmetric probability density function (PDF) of the timing of maximal observable values.[30]

One can estimate the EPR for discrete[31] and continuous systems[32–34] given that all out-of-equilibrium system variables are accessible; otherwise, the EPR estimation becomes challenging,[35–39] and the best estimate would be a lower bound on the total EPR value. Several studies focused on the fluctuations of the EPR calculated from partial information.[40–48] The mathematical relations that bound the EPR using the fluctuations of time asymmetric and generic variables are known as the thermodynamic uncertainty relation (TUR)[49–54] and kinetic uncertainty relation (KUR),[55] respectively. These relations have also been generalized for semi-Markov processes.[56,57] Recently, a unified relation considering both thermodynamic and kinetic quantities has been proposed.[58–60] For systems with partial information, estimators like the passive partial entropy production[47,61,62] and the informed partial entropy production[61–64] are helpful to get a dissipation bound; however, these fail to provide a tight bound on the total EPR for vanishing net current. These average partial entropy production estimators satisfy fluctuations theorems, and as such, they can be derived as a Kullback–Leibler divergence between the forward trajectory and the backward trajectory under auxiliary dynamics.[61]

The k-variable irreversibility measure is defined as, $\sigma_k \equiv k_B \lim_{t\to\infty} \frac{1}{t} D[P(\Gamma^k) \parallel \tilde{\Gamma}^k)]$, where k_B is the Boltzmann constant, $D[p\|q]$ denotes the Kullback–Leibler divergence (KLD)[65,66] between two probability distributions p and q, defined by $D[p \parallel q] = \int \mathrm{d}x p(x) \log(p(x)/q(x))$ and calculated on the positive support.[66] It is a measure of distinguishability[67] between two probability distributions, being non-negative in general and zero for identical distributions. Γ^k denotes the forward path of k nonequilibrium variables for a time duration t, whereas $\tilde{\Gamma}^k$ denotes the corresponding backward path. Owing to the chain-rule of the relative entropy,[68] the more nonequilibrium variables (larger k) included in the path probability measure, the better the KLD bound is, *i.e.*, $0 \le \sigma_1 \le \ldots \le \sigma_k \le \sigma_{k+1} \le \ldots \le \sigma_{\mathrm{tot}}$ where σ_{tot} is the total EPR calculated by the KLD between the forward and reverse trajectories with all the nonequilibrium degrees of freedom.[69,70] Obtaining a tight bound for a continuous variable system using the KLD estimator is challenging since some of the nonequilibrium variables may be inaccessible and sampling the distribution of paths becomes difficult.

In a recent study,[71] Roldan *et al.* transformed the forward and backward time series data of an observed variable of a continuous hair bundle system into two independent and identically distributed time series using a whitening approximation to estimate the KLD from two univariate distributions. They first calculated the EPR bound using only the observed degree of freedom, *i.e.*, the tip position of the hair bundle. Moreover, they used the finite time thermodynamic uncertainty relation to obtain a lower bound on the total EPR using two observables, the tip position and the transduction current, and found a better lower bound on the EPR compared to the one calculated using only one variable, as expected. The EPR estimate calculated with only one observed degree of freedom was typically three orders of magnitude smaller than the total EPR. However, using two observables and the TUR, their measure was three orders of magnitude better than their single-variable result for the oscillatory regime and few fold smaller than the total EPR, but in the quiescent regime, the result was three orders of magnitude smaller than the total EPR.

An estimator based on the KLD between waiting time distributions of the time forward and the time backward transitions between discrete states was shown to provide a lower bound on the total EPR,[64] given that the time-reversal operator does not lead to kinetic hysteresis.[72–75] Applied to a second-order semi-Markov process, this KLD estimator of the EPR breaks into two contributions,[64] the affinity EPR, EPR_{aff}, which accounts for the net flux and affinity or the thermodynamic force,[68,70] and the waiting-time-distribution (WTD) EPR, EPR_{WTD}, which accounts for the broken time-reversal symmetry in the waiting time distributions.[64] For second-order semi-Markov processes, which naturally emerge when "lumping" adjacent states,[64,76] the EPR_{WTD} can provide a lower bound on the total EPR, even when the system does not have any net current observed and $EPR_{aff} = 0$. Describing processes by transitions instead of states,[77] the KLD estimator for the EPR was further applied to waiting times in between observed transitions.[75,78]

Skinner *et al.* presented new estimators to obtain the lower bound on the entropy production rates using optimization techniques.[79,80] They found an estimator given observables characterizing one-step transitions and two successive transitions, whereas in another publication the authors proposed an estimator given the observed waiting time distributions.[80]

There are several studies on the effect of coarse-graining (CG) on the EPR estimation[81–94] specifically discussing whether the CG procedure preserves the EPR fluctuations or not. In a recent study, using a Markovian model of a driven molecular motor, Hartich *et al.* compared different coarse-graining schemes, "milestoning" and "lumping", and found that the "milestoning" method can restore Markovian dynamics in the case of time-scale separation and preserves local detailed balance.[76,86]

The quantitative effect of the coarse-graining on the EPR was estimated in an experimental system of steady-state trajectories of a microtubule length using an optimization procedure of a two-step estimator, where it was demonstrated that increasing the spatial and temporal resolution while coarse-graining leads to an improved EPR bound.[79] Moreover, a recent study by Tan *et al.*[95] has found that the time-irreversibility varies non-monotonically with

the lag time, *i.e.*, the time intervals between the position measurements, which determines the dissipation timescale.[95]

Here, we quantify the irreversibility using a non-invasive method to provide a lower bound on the total EPR in a partially observed model system with continuous variables following oscillatory dynamics, where one of its observables is coarsegrained into a few discrete states. We simulate an oscillating hair-bundle model in which the bundle's tip position is experimentally observed, whereas the position of the molecular motor is hidden. The coarse-grained process follows second-order semi-Markov statistics in the reduced state space (tip position variable space). In this model, the affinity entropy production contribution vanishes; therefore, the irreversibility information can only be accessed from the asymmetries of the waiting time distributions of the forward and the reversed transitions. After the decimation, we exploit the underlying broken time-reversal symmetry stemming from the difference in the PDFs of the waiting times for the upward and the corresponding downward transitions among different coarsegrained states, to calculate the EPR bound, EPR_{WTD}, by applying the KLD estimator. We show that the ratio of the means of the dwell time PDFs of the forward and reverse trajectories, termed the mean dwell-time asymmetry factor, can qualitatively detect the broken time reversal symmetry, and its variation with the number of coarse-grained states is studied. We further calculate the ratio between the EPR_{WTD} and the total EPR as a function of the number of coarse-grained states to evaluate the tightness of the lower bound, and find that with finer resolution (larger number of coarse-grained states), the EPR_{WTD} provides a better lower bound on the dissipation rate.

The paper is organized as follows. First, we introduce the model system and outline the calculation of the total EPR. Then, we describe our coarse-graining procedure, second-order semi-Markovian dynamics of the coarse-grained system, different contributions to the EPR, and mean dwell-time asymmetry factor in the next section. Subsequently, the effect of coarse-graining on the broken time-reversal symmetry, the EPR estimate, and the tightness of the lower bound as a function of the number of coarse-grained states are discussed. Finally, we summarize and provide a future outlook.

2 Model system

We estimate the entropy production rate in a partially observed system described by a Langevin equation. To do so, we consider a model which captures the experimental observation of spontaneous oscillations of mechanosensory hair bundles of auditory hair cells.[71,96–100] These oscillations help to amplify the sound stimuli in the ear of vertebrates, and provide sensitivity and frequency selectivity. Moreover, these oscillations are known as "active" oscillations, and they are distinct from "passive" oscillations that are obtained by blocking the corresponding transduction ion channels.[71] The activity originates from various molecular motors, which cannot be experimentally accessed. However, another degree of freedom coupled to the activity of the molecular motors – the tip position of the hair bundle (X_1) is experimentally observed. Due to the presence of activity, the system is out-of-equilibrium, and its dynamics is governed both by a conservative force $V(X_1,X_2)$, where X_2 represents the position of the center of mass of the molecular motors, and a

non-conservative driving force, $F_{act}(X_1,X_2)$. The system can be described by the following coupled stochastic differential equations.[71,96–98]

$$\lambda_1 \dot{X}_1 = -\frac{\partial V(X_1, X_2)}{\partial X_1} + \sqrt{2k_B T \lambda_1}\xi_1 \quad (1)$$

$$\lambda_2 \dot{X}_2 = -\frac{\partial V(X_1, X_2)}{\partial X_2} - F_{act}(X_1, X_2) + \sqrt{2k_B T_{eff} \lambda_2}\xi_2 \quad (2)$$

where λ_1 and λ_2 are the friction coefficients of the hair bundle tip and the molecular motor, respectively, T and T_{eff} are the environment temperature and the effective temperature characterizing the motor fluctuations, respectively, with ratio $T_{eff}/T > 1$. ξ_1 and ξ_2 are two independent white noise terms with zero-mean and correlation $\langle \xi_i(t)\xi_j(t') \rangle = \delta_{ij}\delta(t - t')$ and k_B is the Boltzmann constant. The functional form of the conservative force, $V(X_1,X_2)$, which is proportional to the difference between the positions of the coupled variables,[96–98] is:

$$V(X_1, X_2) = \frac{k_{gs}\Delta X^2 + k_{sp}X_1^2}{2} - N k_B T \ln\left[e\left(\frac{k_{gs} D \Delta X}{N k_B T}\right) + A\right] \quad (3)$$

where k_{gs} and k_{sp} are the stiffness coefficients, $\Delta X = X_1 - X_2$ is the separation between the position of the hair bundle and the molecular motors, D is the gating swing, and N is the number of transduction channels. $A = \exp[(\Delta G + (k_{gs}D^2)/2N)/(k_B T)]$, and ΔG is the energy difference between the open and closed states of the ion channel. The active non-conservative force exerted by the molecular motors is defined by $F_{act}(X_1,X_2) = F_{max}(1 - SP_0(X_1,X_2))$. The probability of the transduction channel being open is $P_0(X_1,X_2)$, and is defined by $P_0(X_1,X_2) = 1/[1 + A \exp(-k_{gs}D\Delta X/Nk_B T)]$. The non-conservative force depends on the maximum motor force acting on the system (F_{max}), and the calcium-mediated feedback strength (S). The main sources of the non-equilibrium drive come from the ratio T_{eff}/T being greater than unity, and the maximal force (F_{max}) exerted by the molecular motors. This model[71,96–98] was shown to agree well with experimental results.

First, we numerically solve the coupled differential equations (eqn (1) and (2)) for a fixed ratio between the effective temperature and the temperature of the environment ($T_{eff}/T = 1.5$), and different values of S (0.5, 1, 1.5) and F_{max} (70 pN, 80 pN, 90 pN) to obtain simulated trajectories of the hair bundle tip position and the motor position (see Fig. 1 for details on all the parameters used). Although there is clearly a directional current in the X_1–X_2 plane (Fig. 1a) manifesting the nonequilibrium nature of the process, its signature is not obviously present in the trajectories of X_1 or X_2 as a function of time, which oscillate around their respective mean values (as shown in Fig. 1b and c) for a particular set of the driving parameter values, and ESI,† Fig. S1 for additional realizations with different parameters).

As the system is driven out-of-equilibrium by the non-conservative force and the effective temperature, there is a positive dissipation rate. The total entropy production rate can be calculated from the forces and their conjugated currents:[71,101]

$$\mathrm{EPR}_{\mathrm{tot}} = -\left\langle \dot{Q}_1 \right\rangle \left(\frac{1}{T} - \frac{1}{T_{\mathrm{eff}}} \right) + \frac{\left\langle \dot{W}_{\mathrm{act}} \right\rangle}{T_{\mathrm{eff}}} \tag{4}$$

where $\langle \ldots \rangle$ represents the steady state average. The steady state rate of the dissipated heat to the reservoir at temperature T is $\left\langle \dot{Q}_1 \right\rangle = \left\langle (\partial V / \partial X_1) \circ \dot{X}_1 \right\rangle$, with $\circ$ being the Stratonovich product, and $\left\langle \dot{W}_{\mathrm{act}} \right\rangle = -\left\langle F_{\mathrm{act}} \circ \dot{X}_2 \right\rangle$ is the rate of work done by the active force.

3 Coarse-graining, lower bound on the total entropy production rate, and the mean dwell-time asymmetry factor

We used two approaches for spatial coarse-graining to discretize the continuous variable space (the trajectories of the tip position of the hair bundle, X_1) into discrete states: (i) dividing the continuous variable space equally into N (N = 3, 4, 5, 6, 7) coarse-grained states with the ratios 1:1:1, 1:1:1:1, 1:1:1:1:1, 1:1:1:1:1:1, and 1:1:1:1:1:1:1, respectively. This type of equal coarse-graining is only possible for a smooth trajectory for a particular choice of the driving parameter values (Fig. S1, ESI,† *e.g.* F_{max} = 70 pN, S = 1, and F_{max} = 80 pN, S = 1), (ii) diving the continuous variable space into unequal division, where N (N = 3, 4, 5, 6, 7) coarse-grained states correspond to dividing the trajectory with the ratios $1:1:1, 1:\frac{1}{2}:\frac{1}{2}:1, 1:\frac{1}{3}:\frac{1}{3}:\frac{1}{3}:1, 1:\frac{1}{4}:\frac{1}{4}:\frac{1}{4}:\frac{1}{4}:1$ and $1:\frac{1}{5}:\frac{1}{5}:\frac{1}{5}:\frac{1}{5}:\frac{1}{5}:1$, respectively, as shown schematically in Fig. S2 of the ESI.† This type of coarse-graining is better suited to track the irregular oscillations of the tip of the hair cell bundle for driving parameter values F_{max} = 90 pN, S = 1, and F_{max} = 80 pN, S = 1.5, *etc.* (see ESI,† Fig. S1).

We have two layers of coarse-graining: (I) one of the dynamical variables describing the system is decimated (in our example, the tip position of the hair bundle is observed, but the positions of the molecular motor are hidden) (II) we further coarse-grained the observed variable into a few discrete states.

Our system is coarse-grained such that the topology of the coarse-grained system is linear, without any cycles. The probability for a transition between the neighbouring states is non-zero, but the transition probability from one boundary state to the other boundary state is zero, and *vice versa*. For example, in a 3 coarse-grained system (N = 3, 1: 1: 1 spatial division), the probabilities of jumping from macro-state 2 to state 3 or 1 are both non-zero, whereas given the system is in state 1, the probability of finding it in state 3 in the next jump is zero, and *vice versa*. The waiting time distribution of the dwell time at state 2 depends, however, on the state visited before, whether it was state 3 or state 1, rendering the process a second order Markov process. Thus, we consider states composed of the current state, i, and previous state, j, *i.e.*, $[i,j]$ when applying the KLD estimator. Similarly, the approach can be generalized to higher order semi-Markov processes.

Estimating dissipation is non-trivial in the absence of the observable currents or flows, but as dissipated systems exhibit broken time-reversal symmetry, time irreversibility can be exploited to infer the out-of-equilibrium nature of the underlying process from the time series.[64] Martínez *et al.* developed an estimator based on the waiting time distributions

Europe PMC Funders Author Manuscripts

containing information about irreversibility in hidden states even in the absence of visible transitions among the observed states. They applied the technique[64] for a partially hidden network where a subset of states are hidden, and a molecular motor system where the internal states are unresolved. In both cases, their estimator is able to predict a non-zero bound on the entropy production rate at the stalling driving force (the driving parameter value at which the current between the observed states vanishes).

To estimate the lower bound of the irreversibility, we use the KLD estimator,[101,102] which relies on the broken time-reversal symmetry of the underlying waiting-time distributions.[64] Due to the presence of coupled hidden degrees of freedom, the jump process in the observed variable space becomes a second-order[64] semi-Markov. The jump probability depends on the previous state, the time since the last jump, and the final state. The last two conditions make the system direction-time dependent,[91] which means that the joint distribution of times and transitions ($\psi_{nn'}(t)$) cannot be written as a product of the probability distribution for a transition ($\Phi_{nn'}$) and the probability distribution of the time t the system waits at the initial state n ($\psi n(t)$). As proved earlier,[64] the KLD estimator of the EPR for a second-order semi-Markov process consists of two contributions: the affinity EPR ($\mathrm{EPR_{aff}}$) and the waiting-time-distribution EPR ($\mathrm{EPR_{WTD}}$). $\mathrm{EPR_{aff}}$ accounts for the net current and the thermodynamic force of the system. It is sometimes called the "equivalent dissipation".[91] A non-Markovian system and its memoryless counterpart – a system with the same network topology generating a Markovian sequence of states – have the same expression, but, the rate constants are replaced with the effective rate constants for the non-Markovian system. The affinity EPR is written as

$$\mathrm{EPR_{aff}} = \frac{1}{\tau}\sum_{ijk} p(ijk)\ln\frac{p([ij]\to[jk])}{p([kj]\to[ji])} \tag{5}$$

where $p(ijK) = R_{[ij]}p([ij]\to[jk])$ is the probability to observe the sequence $i\to j\to k$. $R_{[ij]}$ denotes the normalized occupancy probability at the CG state j given the previous CG state was i. The numerator and the denominator of the argument of the logarithmic function are of the form $p([ij]\to[jk])$, which denotes the probability that the system makes a transition from a CG state j to a CG state k, given that the previous CG state was i. τ is the mean step duration given by $\tau = \sum_{ij} R_{[i,j]}\tau_{[i,j]}$, where $\tau_{[i,j]}$ is the mean time the system spends at a CG state j, given that the previous CG state was i. The sum is performed over all CG states (i,j, and k). For the active hair bundle system, there is no contribution to the EPR from the affinity EPR, since the coarse-grained system is a linear chain of states.

The other component of the KLD estimator comes from the broken time-reversal symmetry in the waiting-time distributions, and is obtained using the following equation:

$$\mathrm{EPR_{WTD}} = \frac{1}{\tau}\sum_{ijk} p(ijk)D[\Psi(t\mid ijk)\parallel\Psi(t\mid kji)] \tag{6}$$

where $\Psi(t|ijk)$ denotes the probability density function of the time t the system spends at a CG state j before jumping to another CG state k, given that the previous CG state was i, *i.e.*, for $i\to j\to k$ transition. The WTD estimator, $\mathrm{EPR_{WTD}}$, or the "memory dissipation",[91] is

the additional contribution that only exists for non-Markovian systems in contrast to their memoryless Markovian counterpart. It was shown that a semi-Markov process results in non-exponential waiting time distributions,[103] which is related to memory.[91]

Since there is no net current in the observed variable space, the position of the hair-bundle tip, X_1, we use the KLD estimator[64] to calculate a lower bound on the total EPR. In order to apply this estimator, which was developed for discrete states, to a continuous variable system, we coarse-grain the observed variable into a few discrete states (a realization of 3 CG states is shown in Fig. 1d), from which the lower bound is estimated by $\mathrm{EPR}_{\mathrm{WTD}}$, and study how the bound varies as a function of the number of coarse-grained states.

In order to demonstrate that a lower bound on the total EPR can be inferred from the WTD asymmetry in a system with second-order Markov process statistics with a linear topology having zero net current, we use a simple 6-state ($i = 1, 2, 3$ and $i' = 1', 2', 3'$, where states i and i' are indistinguishable) continuous-time Markov chain (CTMC) model coarse-grained into a 3-state linear continuous-time second-order semi-Markov system (observed states $1''$, $2''$, $3''$) as shown in Fig. 2a. The net current in the 6-state model mimics the net current in the X_1–X_2 plane of the active hair bundle model Fig. 1a, whereas the coarse-grained 3-state system resembles the coarse-grained, observed hair-bundle position, X_1. We simulated trajectories using the Gillespie algorithm[104] for 10^8 steps, where after the decimation, we were left with approximately 10^6 jumps. Fig. 2b shows the difference in the distribution of the times the system waits at state $2''$ for an upward transition ($1'' \rightarrow 2'' \rightarrow 3''$) and the corresponding downward transition ($3'' \rightarrow 2'' \rightarrow 1''$). The non-exponential distribution originates from the non-Markovian statistics of the coarse-grained trajectory, whereas the difference between the distributions of the upward and downward waiting times originates from the nonequilibrium nature of the process.[64] Therefore, we can measure the irreversibility from the Kullback–Leibler divergence between the waiting time probability density functions $\mathrm{EPR}_{\mathrm{WTD}}$, for the coarse-grained system with zero $\mathrm{EPR}_{\mathrm{aff}}$ to provide a lower bound on the total EPR.

For example, the waiting time distributions for the hair bundle system at equilibrium ($F_{\mathrm{max}} = 0$ pN, $T = T_{\mathrm{eff}}$) and at nonequilibrium conditions driven according to eqn (1) and (2) are shown in Fig. 3a and b, respectively. The distinguishability between the two WTD in the latter case (b), results in a positive KLD, which bounds the total EPR. The estimation of the $\mathrm{EPR}_{\mathrm{WTD}}$ improves with increasing the number of simulation steps (Fig. 3c) as evident from the decreasing error and the plateauing of the estimation value for the active hair bundle model governed by eqn (1) and (2).[64]

The unimodal nature of the waiting time distributions also refers to the underlying network topology. If a network has internal cycles, the densities could exhibit multimodal behaviour.[75] For a second-order semi-Markov process, the waiting time distributions are direction-time dependent. Thus, the mean dwell-times that the system spends at a particular state for the forward and the reverse transitions are not necessarily identical, and a deviation of their ratio from one provides information regarding the irreversible nature of the process.[80] We calculate the mean dwell-time asymmetry factor (MDAF), *i.e.*, the ratio between the means of the dwell time distributions ($\langle \tau_{k \rightarrow j \rightarrow i} \rangle$ or $\langle \tau_{\mathrm{kji}} \rangle$) of times spent at a

CG state j before transitioning to i, given that it arrived from k, $k \rightarrow j \rightarrow i$, to the mean time the system spends at a CG state j for a $i \rightarrow j \rightarrow k$ transition, ($\langle \tau_{i \rightarrow j \rightarrow k} \rangle$ or $\langle \tau_{ijk} \rangle$). The ratio between the mean times the system spends at a particular state before transitioning to another state and the mean times along the opposite direction ($\langle \tau_{kji} \rangle / \langle \tau_{ijk} \rangle$) being not equal to unity indicates a broken time-reversal symmetry in the system. To obtain the total MDAF for a system with N coarse-grained states, we average the individual MDAF of different transitions among the N coarse-grained states. Therefore, the total MDAF equals $N^{-1} \sum (\langle \tau_{kji} \rangle / \langle \tau_{ijk} \rangle)$. The ratios stemming from the transitions among different coarse-grained states are plotted in the ESI† (Fig. S3).

In the following, we calculate the contribution of the EPR_{WTD} from eqn (6), and the effect of coarse-graining on the EPR and the MDAF, or the time-reversal symmetry breaking.

4 Effect of coarse-graining on the entropy production rate estimation and mean dwell-time asymmetry factor

We exploit the time-reversal symmetry breaking in the coarse-grained system to estimate the EPR. Since the affinity EPR vanishes, the signature of the irreversibility can only be tracked from the KLD between waiting time distributions, EPR_{WTD}.

First, The EPR estimate (EPR_{WTD}) values are calculated using eqn (6) by coarse-graining the X_1 variable into N CG states (where $N = 3, 4, 5, 6, 7$) by equal partitioning of the state space, and plotted as a function of N (Fig. 4a), for $F_{max} = 70$ pN, $S = 1$, and $T_{eff}/T = 1.5$. The lower bound on the EPR estimate is improved with increasing resolution. The maximal value of $EPR_{WTD}/EPR_{tot} = 0.0013$ at 7 coarse-grained states. Moreover, the MDAF is plotted as a function of the number of the coarse-grained states (Fig. 4b).

Next, we calculate the EPR_{WTD} for several driving parameter values ($F_{max} = 70$ pN, $F_{max} = 80$ pN, $F_{max} = 90$ pN, and $S = 0.5, 1, 1.5$) and for unequal spatial spacing of the coarse-grained states ($N = 3, 4, 5, 6, 7$). Both the estimate of the EPR (Fig. 5a) and the mean dwell-time asymmetry factor (Fig. 5b) increase with increasing spatial resolution. Indeed, the EPR estimate is correlated with the MDAF (Fig. 5c), which is related to the non-Markovian nature of the process and the memory involved.[105]

As we mentioned, EPR_{WTD} was calculated for equal (Fig. 4) and unequal (Fig. 5) partitioning of the observed trajectory. For certain driving parameter values at which the trajectories are not that smooth or regular. In that case, the equal partition of the trajectory space of the observed variable would lack enough statistics for the boundary states in the time series. Therefore, we consider unequal spatial partitioning of the trajectory.

To assess the tightness of the bound, we compare the ratio between EPR_{WTD} estimates and the total EPR (EPR_{tot}) calculated for different driving parameter values, $F_{max} = 70$ pN, 80 pN, 90 pN, $S = 0.5, 1, 1.5$, and for different coarse-graining levels (Fig. 6), and find that the tightest bounds is obtained for 7 CG states ($N = 7$), where the EPR_{WTD} values are between 1 to 2 orders of magnitude smaller than the total EPR (Fig. 6). The tightness of the bounds for unequal partitioning for 7 CG states are given in Table S1 of ESI.†

5 Discussion

Most of the previous studies on partially observed systems were performed on Markov chains where some nodes are observed, and the rest are either traced out or lumped together into a hidden state. These processes are performed with the constraints of preserving different quantities (depending on the applied coarse-graining method) like the transition flux among the observed states[93] or preserving the mean value and fluctuations of the entropy production rate at stationary state[87] before and after the coarse-graining. In this paper, we have discussed a different partially observed system where one of the coupled variables following the Langevin dynamics is observed experimentally, and the other is hidden. In addition, we have two layers of coarse-graining, where we preserve the equilibrium density of a particular state before and after the coarse-graining, but due to the linear topology, it cannot support current; therefore, it loses the net current of the original system. We have shown the benefit of using the waiting time distributions in estimating the dissipation rate using the hair bundle cell oscillations as an example. If the edge current vanishes in the observed states, the waiting time distributions may capture the broken time-reversal symmetry in the case of driven systems, depending on the network topology. We infer the irreversibility of the dynamics by coarse-graining the observed system variable into a few discrete states and applying the KLD estimator.[64] The coarse-grained linear system considered in our study is not Markovian, but rather a second-order semi-Markov system, and the breaking of time-reversal symmetry is manifested in the KLD between the non-exponential waiting time distributions of the forward and the reversed transitions among different coarse-grained states.[64] We show that instead of using the full probability distributions, the first cumulants of the dwell time distributions (easier to obtain in experimental scenarios), already provide predictions for the broken time-reversal symmetry and the dissipation rates. This quantity is much easier to quantify, both experimentally and theoretically, serving as a straightforward footprint for time-irreversibility. We further study the mean dwell time asymmetry factor variation with the number of the coarse-grained states.

Berezhkovskii *et al.*[105–108] discussed the case of low-resolution experimental observables in nonequilibrium systems, where the non-Markovian dynamics breaks time-reversal symmetry manifested in differences in the forward and backward waiting times. As suggested by several studies,[105–108] the time asymmetry in the active hair bundle system arises when the following two conditions hold: (i) the reduced variable system follows non-Markovian statistics, and (ii) the system is out-of-equilibrium. Using a 6-state CTMC model which is coarse-grained into a linear 3-state system (Fig. 2), (mimicking the hair cell bundle system with one degree of freedom is decimated), we demonstrate that the resulting waiting time distributions calculated by the Gillespie algorithm[104] show characteristics of second-order semi-Markov statistics, and break time-reversal symmetry under nonequilibrium driving, and thus KLD estimator would be the good choice for the estimation of the EPR. The 6-state network decimated into 3 states mimics the coarse-graining of the X_1 trajectory into 3 coarse-grained states (Fig. 1d), in which a fundamental cycle is lost, and the contribution of the $\mathrm{EPR}_{\mathrm{aff}}$ vanishes. Indeed, we infer a lower bound on the total EPR, which can be calculated from the KLD between the distributions.

We calculate EPR estimates (EPR_{WTD}) of the continuous-space model system, an oscillating hair cell bundle, after coarse-graining the observed X_1 trajectory to equal (Fig. 4a) and unequal (Fig. 5a) spatial divisions. Comparing the results for a particular set of parameter values, F_{max} = 70 pN, S = 1, and T_{eff}/T = 1.5, for which the trajectory is rather smooth and regular (see ESI,† Fig. S1). For the equal and unequal coarse-graining, the lower bounds on the total EPR (*i.e.*, EPR_{WTD}/EPR_{tot}) are 0.0013, and 0.0024, respectively at parameter values F_{max} = 70 pN, S = 1, and T_{eff}/T = 1.5.

The tightness of the lower bounds on the total EPR, *i.e.*, EPR_{WTD}/EPR_{tot}, is found to be 0.0013 for equal spatial division (Fig. 4a) for N = 7 CG state at parameter value F_{max} = 70 pN, S = 1, and T_{eff}/T = 1.5. Whereas, for unequal spatial division (Fig. 6), EPR_{WTD}/EPR_{tot} equals to 0.1244 for N = 7 coarsegrained states at F_{max} = 80 pN, S = 0.5, T_{eff}/T = 1.5, respectively. The similar values of the EPR_{WTD}/EPR_{tot} ratio results from the smooth nature of the X_1 trajectory at the chosen parameter set (as can be seen from Fig. 1c) in contrast to the other parameter values (ESI,† Fig. S1). Equal spatial division for N = 5, 6, 7 coarse-grained states becomes challenging for parameter values that lead to very rugged trajectories due to the lack of statistics for the boundary states.

The inferred time-irreversibility and the EPR_{WTD} estimate increase with finer spatial resolution, *i.e.*, larger number of CG states. Testing a wide range of parameter values, the EPR_{WTD} is smaller by 1 to 2 orders of magnitude compared to the total ERP for the largest spatial resolution (N = 7) considered and unequal spacing of the observed X_1 trajectory, where the tightest bound, $EPR_{WTD}/EPR_{tot} \sim 0.1244$, is obtained for F_{max} = 80 pN, S = 0.5, and T_{eff}/T = 1.5. All the ratios (EPR_{WTD}/EPR_{tot}) for 7 coarse-grained states are listed in Table S1 in the ESI.†

6 Conclusions

In summary, the hair bundle system was used as a model to study the effect of coarse-graining on the lower bound on the total entropy production rate, and the mean dwell-time asymmetry factor. The lower bound on the EPR was estimated using the underlying broken time reversal symmetry induced by the active force for a system with Langevin dynamics and zero net current along the reduced variable space. This approach can be applied to a system following Langevin dynamics with an arbitrary number of observed and hidden states carrying a net flux which vanishes on the observed state-space to quantify the deviation from thermal equilibrium manifested in the irreversibility of the observed degrees of freedom.

Supplementary Material

Refer to Web version on PubMed Central for supplementary material.

Acknowledgments

G. Bisker acknowledges the Zuckerman STEM Leadership Program, and the Tel Aviv University Center for AI and Data Science (TAD). A. Ghosal acknowledges the support of the Pikovsky Valazzi scholarship. This work was supported by the ERC NanoNonEq 101039127, the Air Force Office of Scientific Research (AFOSR) under award number FA9550-20-1-0426, and by the Army Research Office (ARO) under grant number W911NF-21-1-0101.

The views and conclusions contained in this document are those of the authors and should not be interpreted as representing the official policies, either expressed or implied, of the Army Research Office or the U.S. Government.

Notes and references

1. Jarzynski C. Equalities and Inequalities: Irreversibility and the Second Law of Thermodynamics at the Nanoscale. Annu Rev Condens Matter Phys. 2011; 2: 329–351.
2. Seifert U. Stochastic thermodynamics, fluctuation theorems and molecular machines. Rep Prog Phys. 2012; 75 126001 [PubMed: 23168354]
3. Lucia U, Grisolia G, Kuzemsky AL. Time, irreversibility and entropy production in nonequilibrium systems. Entropy. 2020; 22: 1–12.
4. Parrondo JMR, Van Den Broeck C, Kawai R. Entropy production and the arrow of time. New J Phys. 2009; 11 073008
5. Gomez-Marin A, Parrondo JMR, Van Den Broeck C. The 'footprints' of irreversibility. EPL. 2008; 82 (5) 50002
6. Lynn CW, Cornblath EJ, Papadopoulos L, Bertolero MA, Bassett DS. Broken detailed balance and entropy production in the human brain. Proc Natl Acad Sci U S A. 2021; 118 e2109889118 [PubMed: 34789565]
7. Gnesotto FS, Mura F, Gladrow J, Broedersz CP. Broken detailed balance and non-equilibrium dynamics in living systems: a review. Rep Prog Phys. 2018; 81 066601 [PubMed: 29504517]
8. Lan G, Sartori P, Neumann S, Sourjik V, Tu Y. The energy-speed-accuracy trade-off in sensory adaptation. Nat Phys. 2012; 8: 422–428. [PubMed: 22737175]
9. Prost J, Joanny J-FF, Parrondo JMRR. Generalized fluctuation–dissipation theorem for steady-state systems. Phys Rev Lett. 2009; 103: 1–4.
10. Ritort F. Nonequilibrium fluctuations in small systems: from physics to biology. Adv Chem Phys. 2008; 137: 31–123.
11. Mizuno D, Tardin C, Schmidt CF, MacKintosh FC. Nonequilibrium mechanics of active cytoskeletal networks. Science. 2007; 315: 370–373. [PubMed: 17234946]
12. Manosas M, Ritort F. Thermodynamic and kinetic aspects of RNA pulling experiments. Biophys J. 2005; 88: 3224–3242. [PubMed: 15764661]
13. Battle C, Broedersz CP, Fakhri N, Geyer VF, Howard J, Schmidt CF, MacKintosh FC. Broken detailed balance at mesoscopic scales in active biological systems. Science. 2016; 352: 604–607. [PubMed: 27126047]
14. Muy S, Kundu A, Lacoste D. Non-invasive estimation of dissipation from non-equilibrium fluctuations in chemical reactions. J Chem Phys. 2013; 139 124109 [PubMed: 24089752]
15. Lander B, Mehl J, Blickle V, Bechinger C, Seifert U. Noninvasive measurement of dissipation in colloidal systems. Phys Rev E: Stat, Nonlinear, Soft Matter Phys. 2012; 86: 1–4.
16. Zia RKP, Schmittmann B. Probability currents as principal characteristics in the statistical mechanics of non-equilibrium steady states. J Stat Mech: Theory Exp. 2007. P07012
17. Fodor E, Ahmed WW, Almonacid M, Bussonnier M, Gov NS, Verlhac MH, Betz T, Visco P, Van Wijland F. Nonequilibrium dissipation in living oocytes. EPL. 2016; 116 (3) 30008
18. Fodor É, Nardini C, Cates ME, Tailleur J, Visco P, Van Wijland F. How Far from Equilibrium Is Active Matter? Phys Rev Lett. 2016; 117: 1–6.
19. Loi D, Mossa S, Cugliandolo LF. Effective temperature of active complex matter. Soft Matter. 2011; 7: 3726–3729.
20. Martin P, Hudspeth AJ, Jülicher F. Comparison of a hair bundle's spontaneous oscillations with its response to mechanical stimulation reveals the underlying active process. Proc Natl Acad Sci U S A. 2001; 98: 14380–14385. [PubMed: 11724945]
21. Cugliandolo LF, Kurchan J, Peliti L. Energy flow, partial equilibration, and effective temperatures in systems with slow dynamics. Phys Rev E: Stat Phys, Plasmas, Fluids, Relat Interdiscip Top. 1997; 55: 3898–3914.
22. Shiraishi N. Time-symmetric current and its fluctuation response relation around nonequilibrium stalling stationary state. Phys Rev Lett. 2022; 129 020602 [PubMed: 35867465]

23. Andrieux D, Gaspard P, Ciliberto S, Garnier N, Joubaud S, Petrosyan A. Entropy production and time asymmetry in nonequilibrium fluctuations. Phys Rev Lett. 2007; 98: 98–101.
24. Maes C, Netočný K. Time-Reversal and Entropy. J Stat Phys. 2003; 110: 269–310.
25. Liu Q, Wang J. Quantifying the flux as the driving force for nonequilibrium dynamics and thermodynamics in non-Michaelis-Menten enzyme kinetics. Proc Natl Acad Sci U S A. 2020; 117: 923–930. [PubMed: 31879351]
26. Li J, Horowitz JM, Gingrich TR, Fakhri N. Quantifying dissipation using fluctuating currents. Nat Commun. 2019; 10 1666 [PubMed: 30971687]
27. Gingrich TR, Rotskoff GM, Horowitz JM. Inferring dissipation from current fluctuations. J Phys A: Math Theor. 2017; 50 aa672f
28. Ghanta A, Neu JC, Teitsworth S. Fluctuation loops in noise-driven linear dynamical systems. Phys Rev E. 2017; 95: 1–9.
29. Qian H. Vector field formalism and analysis for a class of thermal ratchets. Phys Rev Lett. 1998; 81: 3063–3066.
30. Mori F, Majumdar SN, Schehr GG. Distribution of the time of the maximum for stationary processes. EPL. 2021; 135 30003
31. Cocconi L, Garcia-Millan R, Zhen Z, Buturca B, Pruessner G. Entropy production in exactly solvable systems. Entropy. 2020; 22: 1–33.
32. Tomé T, De Oliveira MJ. Entropy production in irreversible systems described by a Fokker-Planck equation. Phys Rev E: Stat, Nonlinear, Soft Matter Phys. 2010; 82: 1–10.
33. Tomie T. Entropy production in nonequilibrium systems described by a Fokker-Planck equation. Braz J Phys. 2006; 36: 1285–1289.
34. Seifert U. Entropy production along a stochastic trajectory and an integral fluctuation theorem. Phys Rev Lett. 2005; 95: 1–4.
35. Barrio M, Leier A, Marquez-Lago TT. Reduction of chemical reaction networks through delay distributions. J Chem Phys. 2013; 138 104114 [PubMed: 23514472]
36. Jia T, Kulkarni RV. Intrinsic noise in stochastic models of gene expression with molecular memory and bursting. Phys Rev Lett. 2011; 106: 1–4.
37. Pedraza JM, Paulsson J. Effects of molecular memory and bursting on fluctuations in gene expression. Science. 2008; 319: 339–343. [PubMed: 18202292]
38. Basu A, Chowdhury D. Traffic of interacting ribosomes: effects of single-machine mechanochemistry on protein synthesis. Phys Rev E: Stat, Nonlinear, Soft Matter Phys. 2007; 75: 1–11.
39. Nishinari K, Okada Y, Schadschneider A, Chowdhury D. Intracellular transport of single-headed molecular motors KIF1A. Phys Rev Lett. 2005; 95: 1–4.
40. Ehrich J. Tightest bound on hidden entropy production from partially observed dynamics. J Stat Mech: Theory Exp. 2021. 083214
41. Manikandan SK, Gupta D, Krishnamurthy S. Inferring Entropy Production from Short Experiments. Phys Rev Lett. 2020; 124 120603 [PubMed: 32281844]
42. Kim DK, Bae Y, Lee S, Jeong H. Learning Entropy Production via Neural Networks. Phys Rev Lett. 2020; 125 140604 [PubMed: 33064547]
43. Uhl M, Pietzonka P, Seifert U. Fluctuations of apparent entropy production in networks with hidden slow degrees of freedom. J Stat Mech: Theory Exp. 2018. 023203
44. Kahlen M, Ehrich J. Hidden slow degrees of freedom and fluctuation theorems: an analytically solvable model. J Stat Mech: Theory Exp. 2018. 063204
45. Rao R, Esposito M. Detailed fluctuation theorems: a unifying perspective. Entropy. 2018; 20: 8–11.
46. Polettini M, Esposito M. Effective Thermodynamics for a Marginal Observer. Phys Rev Lett. 2017; 119: 1–5.
47. Shiraishi N, Sagawa T. Fluctuation theorem for partially masked nonequilibrium dynamics. Phys Rev E: Stat, Nonlinear, Soft Matter Phys. 2015; 91: 3–8.
48. Rahav S, Jarzynski C. Fluctuation relations and coarse-graining. J Stat Mech: Theory Exp. 2007; 2007 P09012

49. Shiraishi N. Optimal thermodynamic uncertainty relation in Markov jump processes. J Stat Phys. 2021; 185 (19) 1–5.
50. Horowitz JM, Gingrich TR. Thermodynamic uncertainty relations constrain non-equilibrium fluctuations. Nat Phys. 2020; 16: 15–20.
51. Falasco G, Esposito M, Delvenne JC. Unifying thermodynamic uncertainty relations. New J Phys. 2020. 053046
52. Gingrich TR, Horowitz JM, Perunov N, England JL. Dissipation Bounds All Steady-State Current Fluctuations. Phys Rev Lett. 2016; 116: 1–5.
53. Barato AC, Seifert U. Thermodynamic Uncertainty Relation for Biomolecular Processes. Phys Rev Lett. 2015; 114 158101 [PubMed: 25933341]
54. Koyuk T, Seifert U. Thermodynamic Uncertainty Relation for Time-Dependent Driving. Phys Rev Lett. 2020; 125 260604 [PubMed: 33449796]
55. Di Terlizzi I, Baiesi M, Di Terlizzi I, Baiesi M. Kinetic uncertainty relation. J Phys A: Math Theor. 2018; 52 02LT03
56. Ertel B, van der Meer J, Seifert U. Operationally Accessible Uncertainty Relations for Thermodynamically Consistent Semi-Markov Processes. Phys Rev E. 2022; 105 044113 [PubMed: 35590600]
57. Van Vu T, Hasegawa Y. Generalized uncertainty relations for semi-Markov processes. J Phys: Conf Ser. 2020; 1593 012006
58. Vo VT, Van Vu T, Hasegawa Y. arXiv preprint. 2022; arXiv:2203.11501v2 [cond-mat.stat-mech] doi: 10.48550/arXiv.2203.11501
59. Pal A, Reuveni S, Rahav S. Thermodynamic uncertainty relation for first-passage times on Markov chains. Phys Rev Res. 2021; 3: 1–6.
60. Pal A, Reuveni S, Rahav S. Thermodynamic uncertainty relation for systems with unidirectional transitions. Phys Rev Res. 2021; 3 13273
61. Bisker G, Polettini M, Gingrich TR, Horowitz JM. Hierarchical bounds on entropy production inferred from partial information. J Stat Mech: Theory Exp. 2017; 2017 aa8c0d
62. Hartich D, Barato AC, Seifert U. Stochastic thermodynamics of bipartite systems: transfer entropy inequalities and a Maxwell's demon interpretation. J Stat Mech: Theory Exp. 2014. P02016
63. Polettini M, Esposito M. Effective Fluctuation and Response Theory. J Stat Phys. 2019; 176: 94–168.
64. Martínez IA, Bisker G, Horowitz JM, Parrondo JMRR. Inferring broken detailed balance in the absence of observable currents. Nat Commun. 2019; 10: 1–10. [PubMed: 30602773]
65. Terrell GR, Scott DW. Variable Kernel Density. Ann Stat. 1992; 20: 1236–1265.
66. Botev ZI, Grotowski JF, Kroese DP. Kernel density estimation via diffusion. Ann Stat. 2010; 38: 2916–2957.
67. Cover TM, Thomas JA. Elements of Information Theory. 2005.
68. Roldán É, Parrondo JMR. Entropy production and Kullback–Leibler divergence between stationary trajectories of discrete systems. Phys Rev E: Stat, Nonlinear, Soft Matter Phys. 2012; 85: 1–12.
69. Kawai R, Parrondo JMR, Van Den Broeck C. Dissipation: the phase-space perspective. Phys Rev Lett. 2007; 98: 1–4.
70. Roldán I, Parrondo JMR. Estimating dissipation from single stationary trajectories. Phys Rev Lett. 2010; 105: 1–4.
71. Roldan E, Barral J, Martin P, Parrondo JMR, Jülicher F. Quantifying entropy production in active fluctuations of the hair-cell bundle from time irreversibility and uncertainty relations. New J Phys. 2021; 23: 1–16.
72. Hartich D, Godec A. Emergent memory and kinetic hysteresis in strongly driven networks. Phys Rev X. 2021; 11 041047
73. Hartich D, Godec A. arXiv preprint. 2022; doi: 10.48550/arxiv.2112.08978 arXiv:2112.08978v3
74. Bisker G, Martinez IA, Horowitz JM, Parrondo JM. arXiv preprint. 2022; arXiv:2202.02064v1 doi: 10.48550/arxiv.2202.02064

75. van der Meer J, Ertel B, Seifert U. Thermodynamic inference in partially accessible Markov networks: a unifying perspective from transition-based waiting time distributions. Phys Rev X. 2022; 12 031025
76. Hartich D, Godec A. arXiv preprint. 2021; arXiv: 2111.14734v2 [cond-mat.stat-mech] doi: 10.48550/arXiv.2111.14734
77. Harunari PE, Garilli A, Polettini M. arXiv preprint. 2022; arXiv:2205.05060v1 [cond-mat.stat-mech] doi: 10.48550/arXiv.2205.05060
78. Harunari PE, Dutta A, Polettini M, Roldán É. arXiv preprint. 2022; arXiv:2203.07427v2 [cond-mat.stat-mech] doi: 10.48550/arXiv.2203.07427
79. Skinner DJ, Dunkel J. Improved bounds on entropy production in living systems. Proc Natl Acad Sci U S A. 2021; 118 (18) e2024300118 [PubMed: 33906948]
80. Skinner DJ, Dunkel J. Estimating entropy production from waiting time distributions. Phys Rev Lett. 2021; 127 198101 [PubMed: 34797138]
81. Busiello DM, Gupta D, Maritan A. Coarse-grained entropy production with multiple reservoirs: unraveling the role of time scales and detailed balance in biology-inspired systems. Phys Rev Res. 2020; 2 43257
82. Busiello DM, Hidalgo J, Maritan A. Entropy production for coarse-grained dynamics. New J Phys. 2019; 21 073004
83. Bo S, Celani A. Entropy Production in Stochastic Systems with Fast and Slow Time-Scales. J Stat Phys. 2014; 154: 1325–1351.
84. Bo S, Celani A. Multiple-scale stochastic processes: decimation, averaging and beyond. Phys Rep. 2017; 670: 1–59.
85. Esposito M. Stochastic thermodynamics under coarse graining. Phys Rev E: Stat, Nonlinear, Soft Matter Phys. 2012; 85: 1–11.
86. Kawaguchi K, Nakayama Y. Fluctuation theorem for hidden entropy production. Phys Rev E: Stat, Nonlinear, Soft Matter Phys. 2013; 88: 1–5.
87. Teza G, Stella AL. Exact Coarse Graining Preserves Entropy Production out of Equilibrium. Phys Rev Lett. 2020; 125 110601 [PubMed: 32975992]
88. Gomez-Marin A, Parrondo JMR, Van Den Broeck C. Lower bounds on dissipation upon coarse graining. Phys Rev E: Stat, Nonlinear, Soft Matter Phys. 2008; 78: 1–11.
89. Bilotto P, Caprini L, Vulpiani A. Excess and loss of entropy production for different levels of coarse graining. Phys Rev E. 2021; 104: 1–8.
90. Sohn, Jil. An example of temporal coarse-graining of entropy production. Eur Phys J B. 2015; 88: 1–5.
91. Yang X, Chen Y, Zhou T, Zhang J. Exploring dissipative sources of non-Markovian biochemical reaction systems. Phys Rev E. 2021; 103 052411 [PubMed: 34134237]
92. Pigolotti S, Vulpiani A. Coarse graining of master equations with fast and slow states. J Chem Phys. 2008; 128 154114 [PubMed: 18433197]
93. Seiferth D, Sollich P, Klumpp S. Coarse graining of biochemical systems described by discrete stochastic dynamics. Phys Rev E. 2020; 102: 1–17.
94. Celani A, Bo S, Eichhorn R, Aurell E. Anomalous thermodynamics at the microscale. Phys Rev Lett. 2012; 109: 1–4.
95. Tan TH, Watson GA, Chao Y-C, Li J, Gingrich TR, Horowitz JM, Fakhri N. arXiv preprint. 2021; arXiv:2107.05701v1 [physics.bio-ph] doi: 10.48550/arXiv.2107.05701
96. Barral J, Jülicher F, Martin P. Friction from Transduction Channels' Gating Affects Spontaneous Hair-Bundle Oscillations. Biophys J. 2018; 114: 425–436. [PubMed: 29401440]
97. Bormuth V, Barral J, Joanny JF, Jülicher F, Martin P. Transduction channels' gating can control friction on vibrating hair-cell bundles in the ear. Proc Natl Acad Sci U S A. 2014; 111: 7185–7190. [PubMed: 24799674]
98. Tinevez JY, Jülicher F, Martin P. Unifying the various incarnations of active hair-bundle motility by the vertebrate hair cell. Biophys J. 2007; 93: 4053–4067. [PubMed: 17704173]
99. Martin P, Bozovic D, Choe Y, Hudspeth AJ. Spontaneous oscillation by hair bundles of the bullfrog's sacculus. J Neurosci. 2003; 23: 4533–4548. [PubMed: 12805294]

100. Nadrowski B, Martin P, Jülicher F. Active hair-bundle motility harnesses noise to operate near an optimum of mechanosensitivity. Proc Natl Acad Sci U S A. 2004; 101: 12195–12200. [PubMed: 15302928]

101. Dabelow L, Bo S, Eichhorn R. Irreversibility in Active Matter Systems: Fluctuation Theorem and Mutual Information. Phys Rev X. 2019; 9 21009

102. Gaveau B, Granger L, Moreau M, Schulman LS. Relative entropy, interaction energy and the nature of dissipation. Entropy. 2014; 16: 3173–3206.

103. Tu Y. The nonequilibrium mechanism for ultrasensitivity in a biological switch: sensing by Maxwell's demons. Proc Natl Acad Sci U S A. 2008; 105: 11737–11741. [PubMed: 18687900]

104. Xiaodong C. Exact stochastic simulation of coupled chemical reactions with delays. J Chem Phys. 2007; 126: 2340–2361.

105. Shin J, Shin J, Berezhkovskii AM, Kolomeisky AB, Kolomeisky AB, Kolomeisky AB, Kolomeisky AB. Biased Random Walk in Crowded Environment: Breaking Uphill/Downhill Symmetry of Transition Times. J Phys Chem Lett. 2020; 11: 4530–4535. [PubMed: 32433884]

106. Berezhkovskii AM, Makarov DE. On the forward/ backward symmetry of transition path time distributions in nonequilibrium systems. J Chem Phys. 2019; 151 065102

107. Shin J, Berezhkovskii AM, Kolomeisky AB. Crowding breaks the forward/backward symmetry of transition times in biased random walks. J Chem Phys. 2021; 154 204104 [PubMed: 34241169]

108. Berezhkovskii AM, Hummer G, Bezrukov SM. Identity of distributions of direct uphill and downhill translocation times for particles traversing membrane channels. Phys Rev Lett. 2006; 97: 1–4.

Europe PMC Funders Author Manuscripts

Europe PMC Funders Author Manuscripts

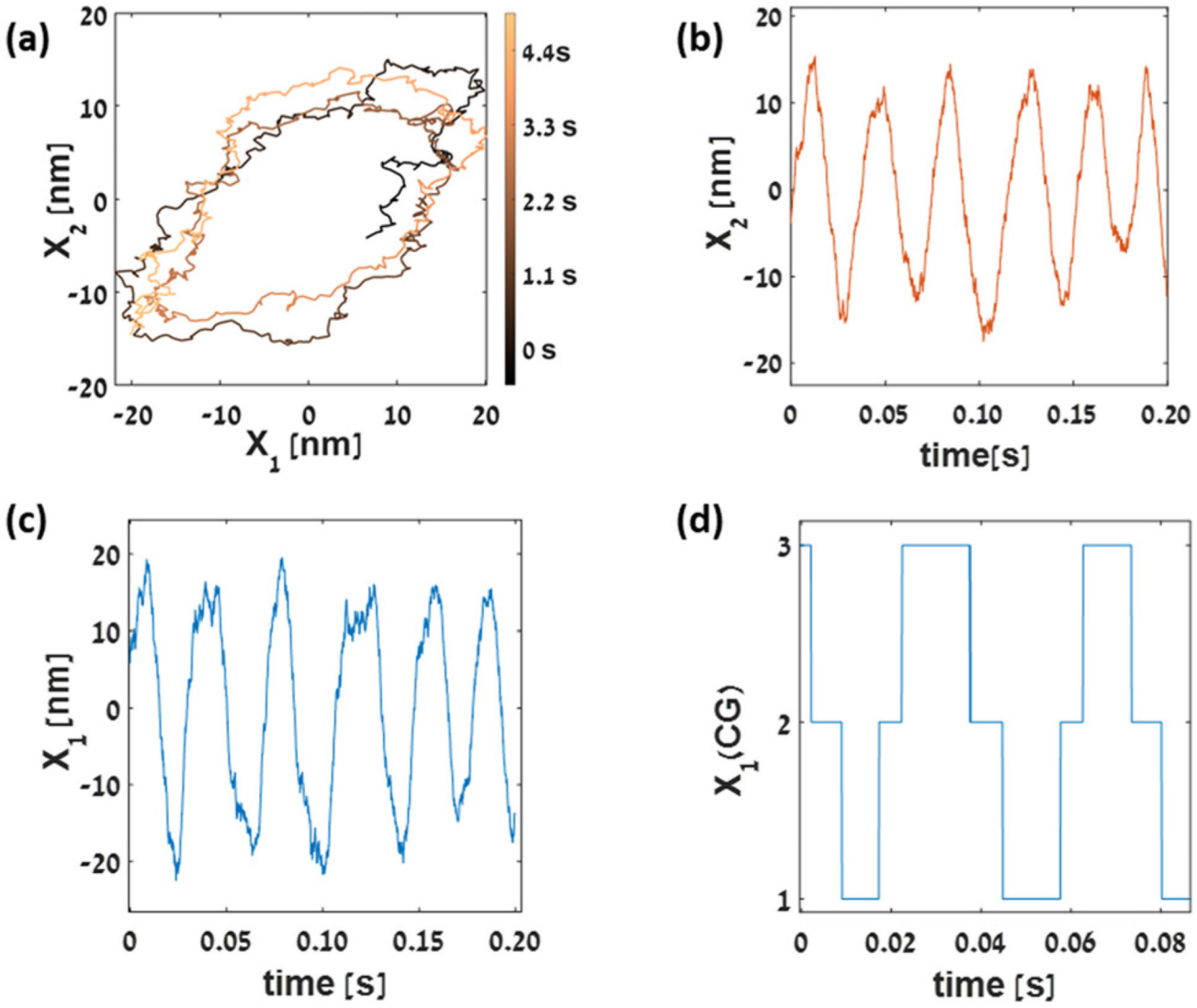

Fig. 1.

Simulated trajectories of the observed (X_1, the tip position of the hair bundle) and the hidden (X_2, the position of the molecular motors) variables and the coarse-grained trajectory of the observed variable after spatial coarse-graining (a) the trajectories in the X_1–X_2 plane for fixed values of driving parameters: (F_{max} = 70 pN, $S = 1$, $T_{eff}/T = 1.5$). The color of the curve represents time going from dark to bright (b) $X_2 = X_2 - \langle X_2 \rangle$, as a function of time for fixed values of driving (F_{max} = 70 pN, S = 1, $T_{eff}/T = 1.5$). (c) $X_1 = X_1 - \langle X_1 \rangle$, as a function of time for the same values of driving parameters, which does not show any sign of net flux, (d) the coarse-grained trajectory for 3 CG states at above mentioned parameter values. All the quantities plotted are calculated for the following additional parameter values: λ_1 = 2.8 pN ms nm^{-1}, λ_2 = 10 pN ms nm^{-1}, k_{gs} = 0.75 pN nm^{-1}, k_{sp} = 0.6 pN nm^{-1}, D = 61 nm, $k_B T$ = 4 pN nm, $\Delta G = 10 k_B T$.

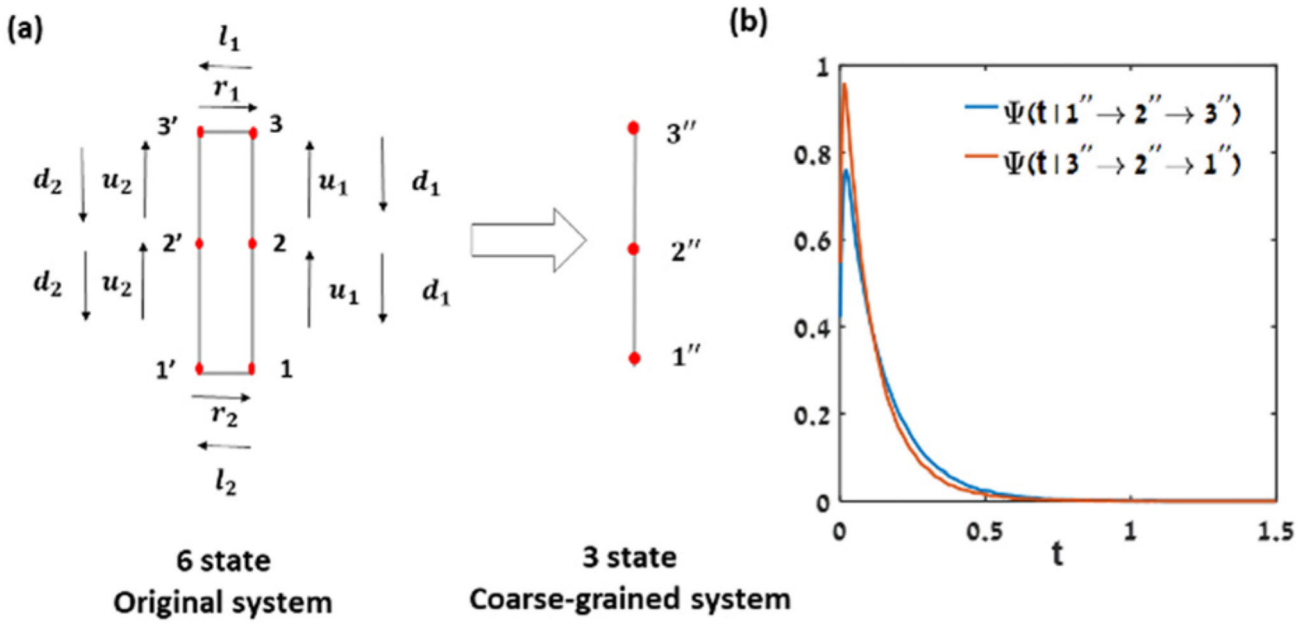

Fig. 2.

The $X_1 - X_2$ trajectory of the hair bundle system coarse-grained into a linear topology in X_1 state space after decimation of the X_2 states with zero net flux motivates to use KLD estimator of the waiting times ($t\,[s]$): (a) The circles with the lines represents a 6 state system, which after decimation is reduced to a linear 3 state system, (b) non-zero contribution from the Kullback–Leibler divergence of the waiting time distributions: the distribution of the waiting times ($t\,[s]$) the system waits at CG state $2''$ for an ($1'' \to 2'' \to 3''$) upward transition (blue solid line) and ($3'' \to 2'' \to 1''$) the downward transition (red solid line) for the following parameter values: $u_1 = 10$, $u_2 = 3$, $d_1 = 2$, $d_2 = 4$, $r_1 = 3$, $r_2 = 3$, $l_1 = 1$, $l_2 = 1$.

Europe PMC Funders Author Manuscripts

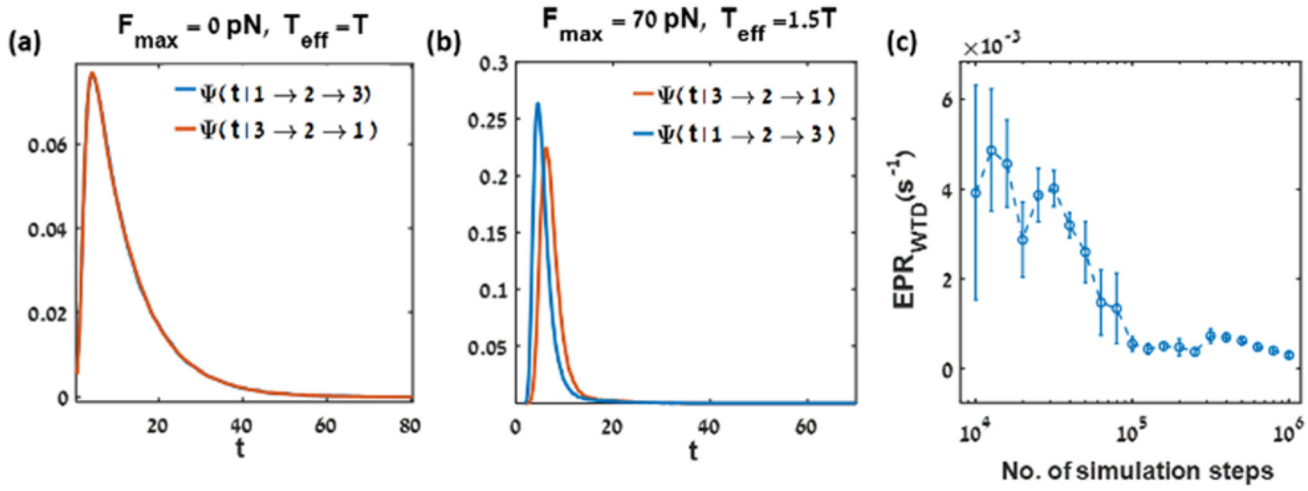

Fig. 3.

Entropy production rate estimation from the Kullback–Leibler divergence between the waiting time distributions for 3 equally spaced coarse-grained states of the active hair bundle's tip position: probability density functions of the time (t [s]) that the system stays at state 2 for an upward transition (blue solid line), and for a downward transition (red solid line) for two different parameter values: (a) F_{max} = 0 pN, T_{eff} = T, and S = 1.5, (b) $F_{max\times}$ = 70 pN, T_{eff} = 1.5 T, and S = 1.5, (c) EPR_{WTD}. as a function of length of the simulation for F_{max} = 70 pN, T_{eff}/T = 1.5, and S = 1.5. The error bar at each point describes the standard error of the mean.

Europe PMC Funders Author Manuscripts

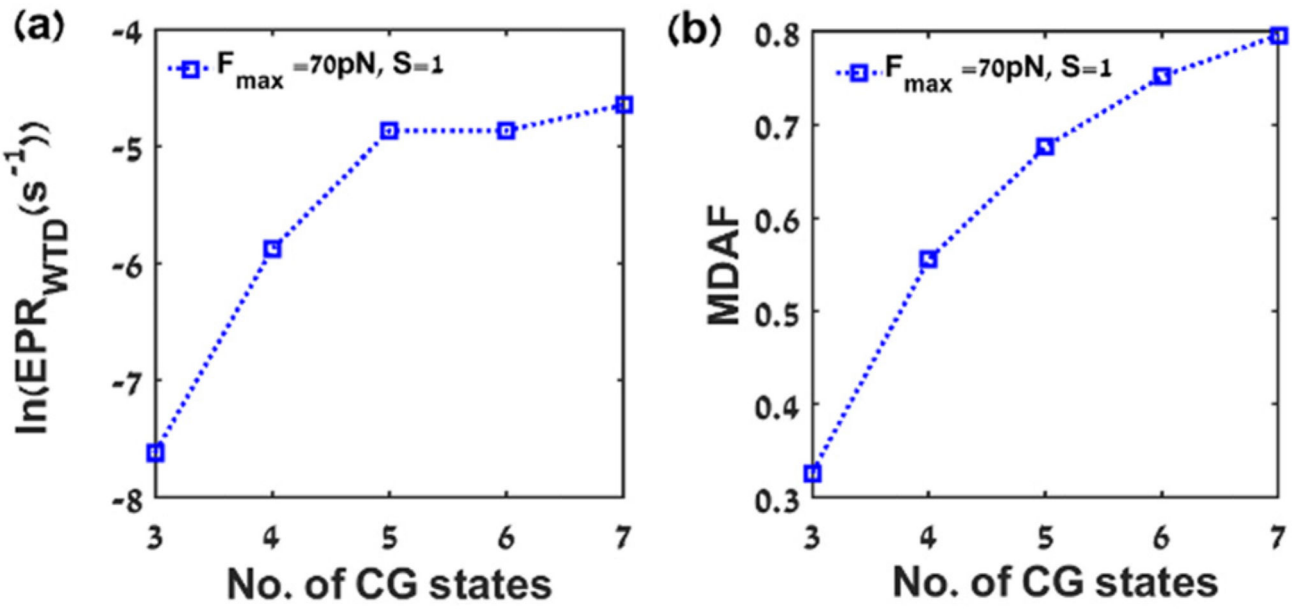

Fig. 4.

Entropy production rate estimation and the mean dwell-time asymmetry factor (MDAF) for equal spacing coarse-graining of X_1 trajectory: (a) EPR_{WTD} (s^{-1}) (WTD estimate of the EPR) as a function of the number of CG states with equal spacing for parameter values F_{max} = 70 pN, S = 1, and T_{eff}/T = 1.5 (b) MDAF (mean dwell-time asymmetry factor) as a function of the number of CG states. The other parameter values are the same as mentioned in Fig. 1. The lines are drawn to as a guide to the eye. The total EPR for this set of parameter values is 7.3312 s^{-1}.

Europe PMC Funders Author Manuscripts

Europe PMC Funders Author Manuscripts

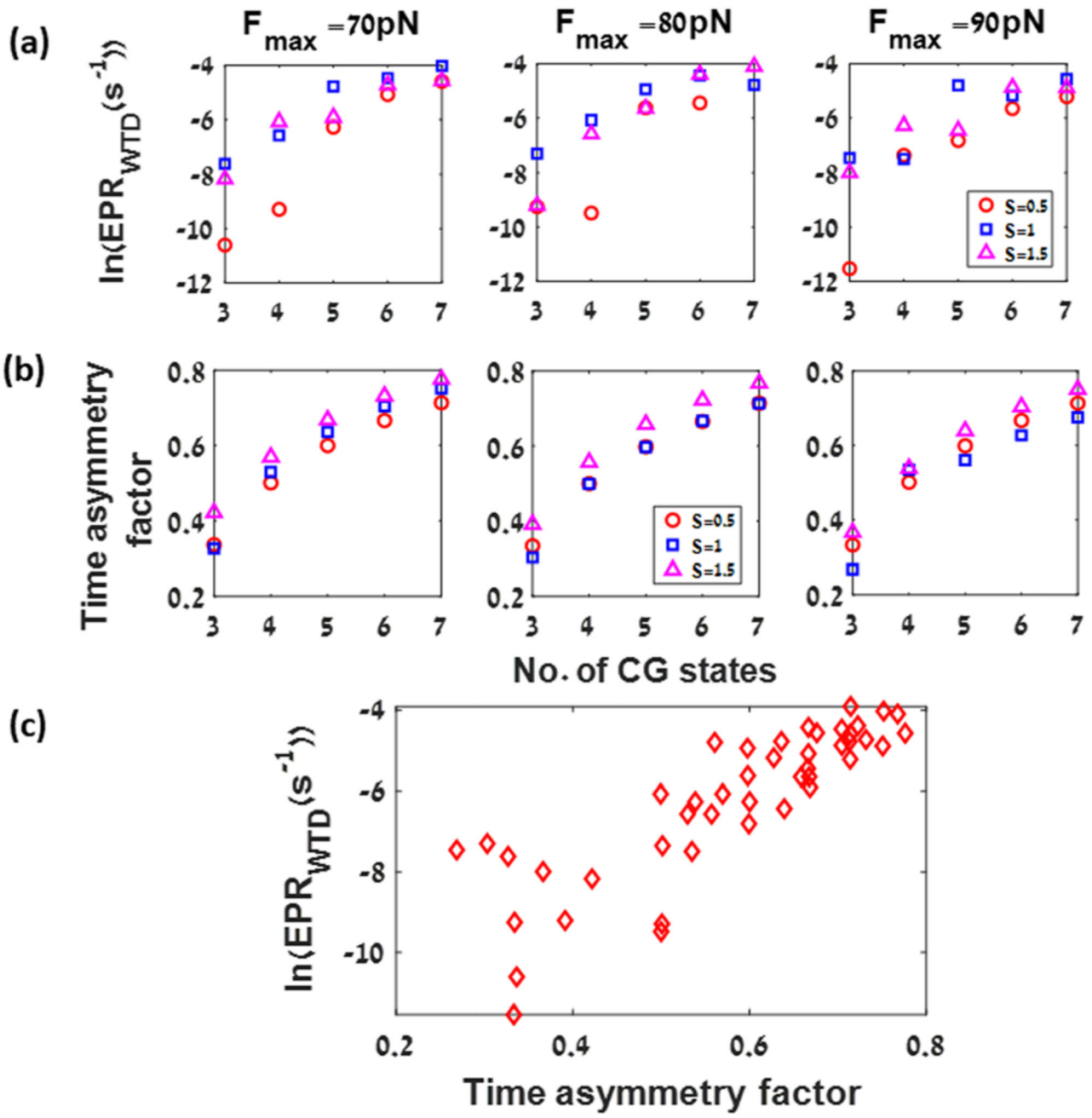

Fig. 5.

Effect of coarse-graining on the EPR_{WTD} (s^{-1}) and the mean dwell-time asymmetry factor (MDAF): (a) EPR_{WTD} (s^{-1}) as a function of number of CG states (3 CG: 1:1:1, 4 CG: 1:1/2:1/2:1, 5 CG: 1:1/3:1/3:1/3:1, 6CG:1:1/4:1/4:1/4:1/4:1, and 7CG: 1:1/5:1/5:1/5:1/5:1/5:1) for different parameter values, (left) F_{max} = 70 pN for S = 0.5, 1, 1.5, (middle) F_{max} = 80 pN for S = 0.5, 1, 1.5, and (right) F_{max} = 90 pN, S = 0.5, 1, 1.5. (b) The MDAF as a function of number of CG states for different parameter values: (left) F_{max} = 70 pN, S = 0.5,1,1.5; (middle) F_{max} = 80 pN, S = 0.5, 1, 1.5; (right) F_{max} =

90 pN, $S = 0.5, 1, 1.5$. In both panels: red circle symbols correspond to $S = 0.5$, blue square symbols correspond to $S = 1$, and magenta triangle symbols correspond to $S = 1.5$. (c) The values of EPR_{WTD} as a function of the MDAF for all transitions and all parameter values as mentioned earlier. The other parameter values used in these figures are mentioned in Fig. 1.

Europe PMC Funders Author Manuscripts

Europe PMC Funders Author Manuscripts

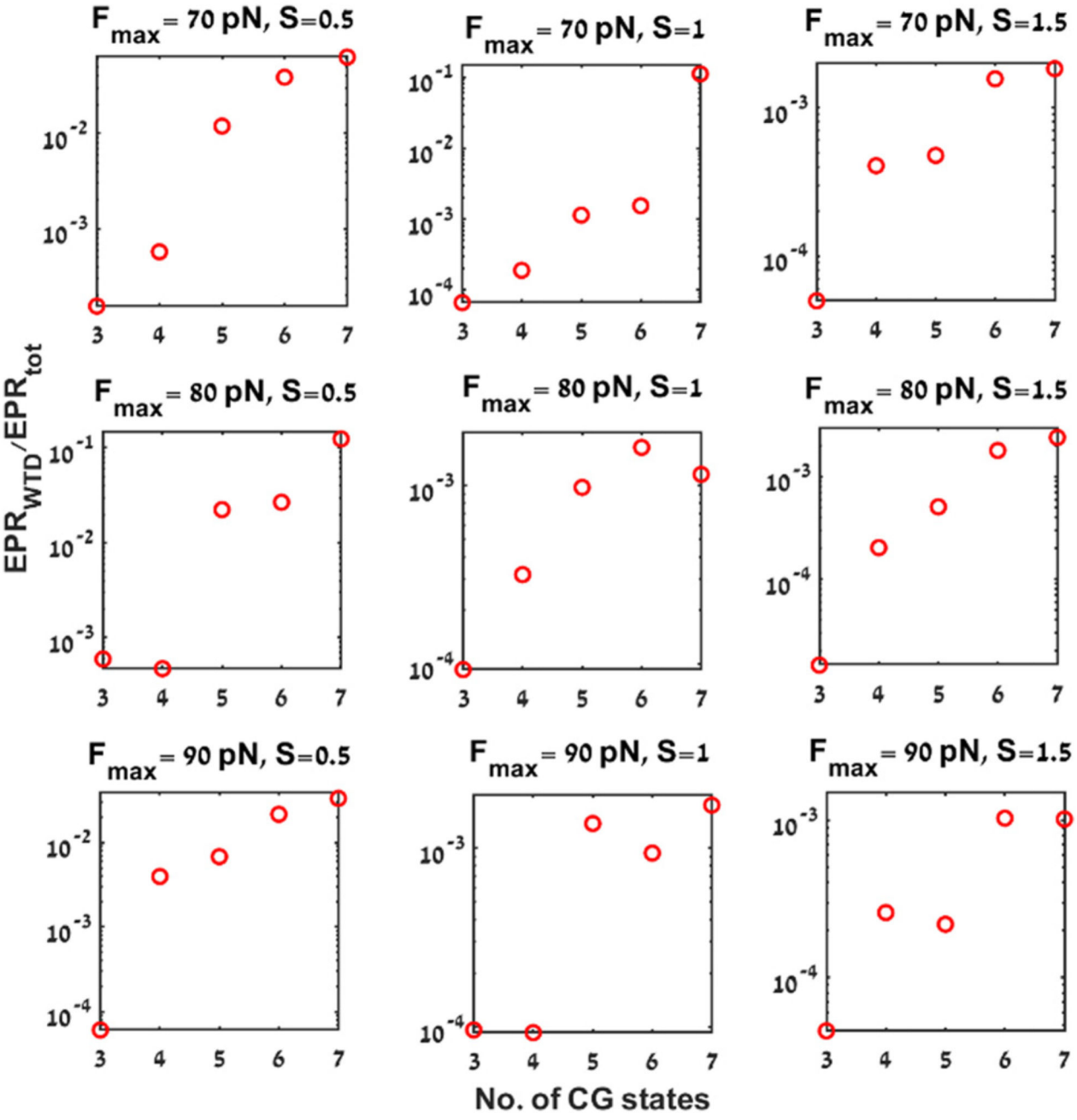

Fig. 6.

Tightness of the EPR bound (EPR_{WTD}) as a function of number of CG states: ratio between the EPR estimates from the waiting time distribution (EPR_{WTD} (s^{-1})) and the total entropy production rate (EPR_{tot} (s^{-1})) for different parameter values. The coarse-graining corresponds to unequal divisions of the X_1 state space. The parameter values are F_{max} = 70 pN, S = 0.5, 1, 1.5 (upper row), F_{max} = 80 pN, S = 0.5, 1, 1.5 (middle row), F_{max} = 90 pN, S

= 0.5, 1, 1.5 (lower row). The other parameter values used in this figure are as mentioned in Fig. 1.

Europe PMC Funders Author Manuscripts